Elastic and inelastic scattering of oxygen ions from nickel and germanium isotopes

M. E. Cobern,* N. Lisbona, and M. C. Mermaz
Département de Physique Nucléaire, C.E.N. Saclay, BP 2, 91190 Gif sur Yvette, France
(Received 1 October 1975)

The elastic and inelastic cross sections for the scattering of $^{16,18}O$ ions from targets of $^{72,74,76}Ge$ and of ^{16}O from ^{64}Ni have been measured at a laboratory energy of 56 MeV. The angular distributions for the ground and first-excited (2^+) levels have been analyzed simultaneously by a coupled-equations search routine, and optical potentials determined. It is shown that this method reduces the ambiguity in the potentials.

[NUCLEAR REACTIONS ^{64}Ni, $^{72,74,76}Ge(^{16}O, ^{16}O')$, $^{72,74,76}Ge(^{18}O, ^{18}O)$, and $(^{18}O, ^{18}O')$; measured $\sigma(\theta)$, $E = 56$ MeV; coupled equations analysis; derived 6-parameter optical potentials, deformation parameters.]

I. INTRODUCTION

One of the problems faced in the analysis of heavy-ion induced transfer reactions is the lack of accurate optical potentials for distorted-wave Born approximation (DWBA) or coupled-channels Born approximation (CCBA) calculations. There are two main difficulties with these potentials, which may be summarized as follows

(i) *Ambiguities.* It has long been known that for heavy-ion, or even α-particle, scattering the elastic cross section alone is insufficient to completely determine the potential parameters.[1,2] Even in the case of a restricted four-parameter (i.e., equal geometry) potential, the parameters are correlated by the "Igo ambiguity".[1] The situation is further complicated by the fact that such equal geometry potentials are often unable to reproduce the observed transfer angular distributions, making it necessary to introduce additional parameters, and hence, greater ambiguity, in order to provide the required "surface transparency." This transparency can be created either by an imaginary potential whose radius and diffusivity are smaller than those for the real potential[3,4] (a six-parameter fit), or by the combination of a small, sharp volume, and broad surface-derivative absorption[5] (in effect, a seven-parameter potential.)

(ii) *Inclusion of inelastic effects.* In the simple optical model, an imaginary potential is employed to represent macroscopically all of the interactions that can draw off flux from the elastic channel; each individual route is assumed to be weak compared to elastic scattering.[6] This last assumption is less valid in heavy-ion reactions, particularly where there is strong intraband coupling in a vibrational or rotational target nucleus. Then, strong inelastic excitations can perturb the elastic scattering angular distributions, via multistep processes. In such cases, the use of a CCBA code is necessary to treat transfer reactions resulting from this channel. The use, in such a calculation, of a potential derived purely from an optical model analysis of elastic scattering is erroneous. The inelastic excitation is double counted: once explicitly in the coupled channels formalism, and once implicitly in the derived imaginary potential.

In an attempt to resolve these two problems, we have studied the elastic and inelastic scattering of ^{16}O ions at 56 MeV by targets of ^{64}Ni and $^{72,74,76}Ge$, as well as ^{18}O scattering from the germanium isotopes. The measured angular distributions were analyzed with the sequential-iteration coupled equations code ECIS,[8] which allows a least-squares search for parameters to reproduce the ground and excited states simultaneously. The experimental procedures are discussed in Sec. II, and the analysis in Sec. III A. Section III B deals with some general features of the calculations, and in particular, the effect of Coulomb-nuclear interference. Section III C treats the question of ambiguities.

II. EXPERIMENTAL METHOD

A 56 MeV beam of either ^{16}O or ^{18}O ions from the Saclay FN tandem accelerator was scattered from isotopically enriched targets of ^{64}Ni and $^{72,74,76}Ge$ on 20 $\mu g/cm^2$ carbon backing. Thin (~50 $\mu g/cm^2$) targets were necessary to prevent their destruction by excessive heating due to beam energy loss.

The elastically and inelastically scattered particles were detected in three 100 μm Si (S.B.) detectors, with measurements made in 2.5° steps from 12.5° to 70°, and at 80°, 90°, and 100° (lab-

oratory angle). Particle identification was unnecessary due to the negative Q values for the important reaction channels. A monitor detector permitted the normalization between runs, and the solid-angle ratios for the three detectors were determined by comparing elastic cross sections measured at the same angle. The absolute normalization was determined by averaging the ratio to the Rutherford cross section at several forward angles, where the scattering is purely Coulomb, and setting this average to unity. This over-all normalization is estimated to be accurate to ±6%.

Because of the resolution of the detector system (~220 keV), it was extremely difficult, particularly at forward angles, to extract the inelastic cross section from the large tail of the elastic peak. For this reason, many of the measurements were repeated using a Buechner single-gap spectrograph and a position-sensitive surface-barrier detector. A typical position spectrum is shown in Fig. 1, indicating an energy resolution of 120 keV full width at half-maximum (FWHM). Due to the presence of multiple charge states of the outgoing ions, whose distribution is energy dependent, the number of counts for the inelastic peak, N_2 was determined by the formula

$$N_2 = N_2^{\text{meas}} \times \sigma_{\text{el}}\,(\text{detector})/\sigma_{\text{el}}(\text{spectrograph})\,.$$

Since the excitation energy of the 2^+ levels are 600 keV for all of the isotopes, the charge-state distributions should be the same as those for the ground states. At extreme forward angles, there was occasionally a contaminant peak due to the presence of different charge states and ion species (e.g., $^{16}N^{7+}$). Since, for the same value of $B\rho$, the energy of these particles was different, it was possible to integrate the area of the contaminant peak in the energy spectrum and subtract it from the measured position spectrum.

The experimental results, with the best-fit calculations (see Sec. III A), are shown in Figs. 2–6. Figures 2 and 3 represent the cross sections for the elastic scattering of ^{16}O and ^{18}O, respectively, by the germanium isotopes, divided by the Rutherford cross section. The inelastic cross sections for the first 2^+ levels are shown in Figs. 4 and 5. The elastic and inelastic angular distributions for $^{16}O + {}^{64}Ni$ scattering are shown in Fig. 6. The error bars indicated include the uncertainty in the over-all normalization.

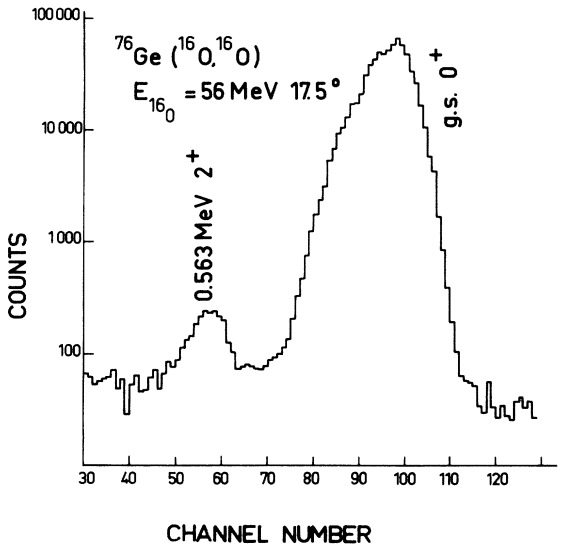

FIG. 1. Typical position spectrum of the position-sensitive detector PSD in Buechner spectrometer. Resolution is about 120 keV (FWHM).

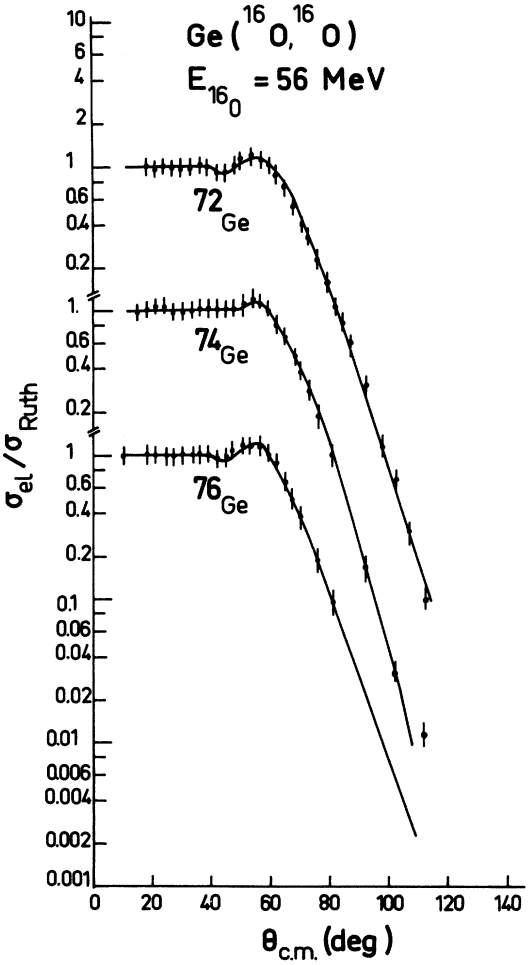

FIG. 2. Ratio of elastic to Rutherford cross sections for the $^{16}O + Ge$ systems. Solid curve represents the result of the ECIS fit using the parameters given in Table I. Error bars include 6% uncertainty in absolute normalization.

III. ANALYSIS

A. Coupled-equations analysis

For the analysis of the elastic and inelastic cross sections, the coupled-equations code, ECIS, written by Raynal, was employed.[8] This program utilizes a sequential-iteration method to solve the coupled equations, starting from a first-order solution which is similar to the DWBA result. The convergence of the iterations is accelerated, and possible instabilities suppressed, by the use of Padé approximants.[9]

The program includes the means for a least-squares search on the optical model and deformation parameters to minimize the total (i.e., elastic and inelastic) χ^2 value. Since these parameter searches are costly and time consuming, however, an extensive survey over a grid of starting values was not feasible. We therefore chose a few potentials reported for various heavy-ion reactions[3,10] as starting points for the search on the $^{16}O+^{74}Ge$ system. The search was carried out alternatively on two groups of parameters: (V_0, a_V, r_W, β_2) and (W_0, a_W, r_V, β_2). This procedure was necessitated by the limitation on the number of search parameters in the code. (In all of the searches, the Coulomb radii were fixed to those for the real nuclear potential.) The best values

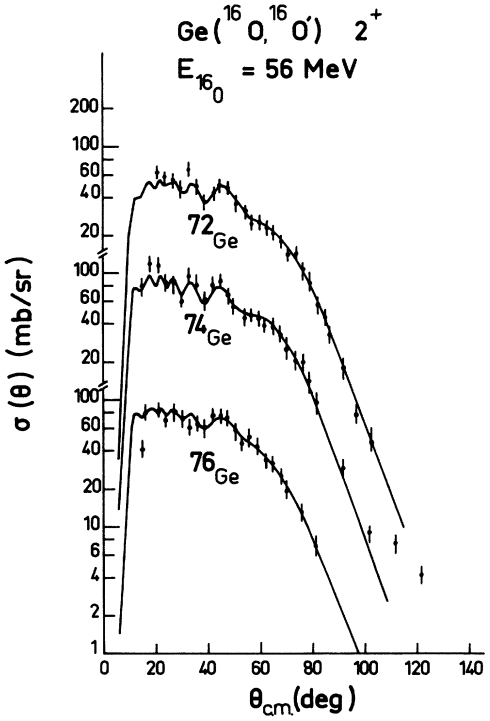

FIG. 4. Inelastic cross sections for Ge(^{16}O, ^{16}O′)-Ge(2_1^+). See caption to Fig. 2.

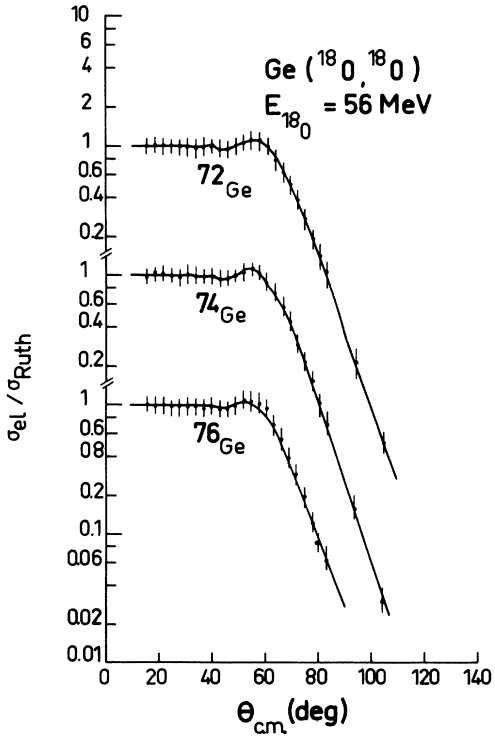

FIG. 3. Elastic angular distributions for the $^{18}O+Ge$ systems. See caption to Fig. 2.

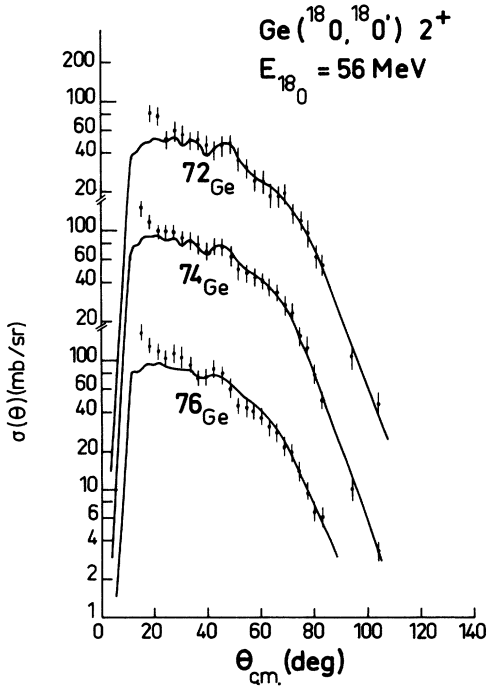

FIG. 5. Inelastic cross sections for Ge(^{18}O, ^{18}O′)-Ge(2_1^+). See caption to Fig. 2.

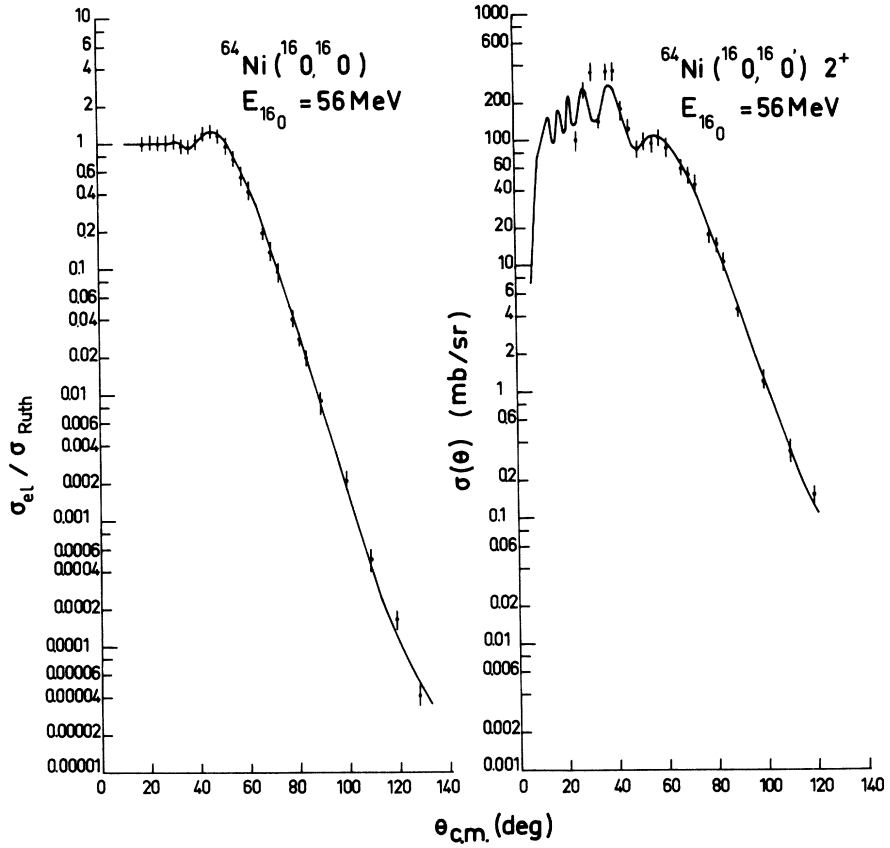

FIG. 6. Elastic and inelastic cross sections for $^{16}O + ^{64}Ni$ scattering. See caption to Fig. 2. The scale in mb/sr has to be divided by 10.

found were then used as a starting point for the other combination of target and projectile. (The "family" chosen gave significantly better results than the others tried.) The potentials found by this search procedure are listed in Table I; Table II lists the values of β_2 and compares them with the published values from Coulomb excitation.[11]

Several general features of these potentials should be noted. First, they all display to varying degrees a surface transparency,[5] in that the radius and diffusivity of the imaginary part of the potentials are smaller than the corresponding values for the real part. Second, these are all rather shallow potentials; no deep potential gave nearly as good a fit. Finally, it can be seen that the diffusivities are, in general, larger for the case of ^{18}O scattering than for ^{16}O, in order to reproduce the observed lack of structure in the ^{18}O inelastic cross sections (Fig. 5).

B. Effects of Coulomb excitation and Coulomb-nuclear interference

In the inelastic scattering of heavy ions at tandem energies, Coulomb excitation plays a dominant role. This is due to the large Z_1Z_2 product, as well as the long range of the interaction causing the excitation ($\propto 1/r^3$ for a 2^+ level). The nuclear excitation amplitude interferes strongly and destructively with the Coulomb excitation, due to the opposite signs of the potentials.[10,12] This effect is dramatically presented in Fig. 7, where

TABLE I. Best-fit optical potentials from the coupled-channels analysis:

$$V(r) = V\left[1+\exp\left(\frac{r-R_0}{a_0}\right)\right]^{-1} + W\left[1+\exp\left(\frac{r-R_i}{a_i}\right)\right]^{-1},$$

$$R_0 = r_0(A_T^{1/3} + A_P^{1/3}), \quad R_i = r_i(A_T^{1/3} + A_P^{1/3}).$$

System	V (MeV)	r_0 (fm)	a_0 (fm)	W (MeV)	r_i (fm)	a_i (fm)
$^{64}Ni + ^{16}O$	31.2	1.31	0.50	42.3	1.25	0.37
$^{72}Ge + ^{16}O$	20.4	1.35	0.50	31.6	1.29	0.41
$^{74}Ge + ^{16}O$	24.4	1.36	0.43	36.6	1.27	0.42
$^{76}Ge + ^{16}O$	16.6	1.36	0.49	45.6	1.28	0.37
$^{72}Ge + ^{18}O$	18.4	1.36	0.53	39.2	1.30	0.40
$^{74}Ge + ^{18}O$	21.5	1.34	0.55	27.6	1.31	0.42
$^{76}Ge + ^{18}O$	12.3	1.36	0.64	28.2	1.34	0.45

the Coulomb, real, and imaginary nuclear contributions to the cross section are plotted individually. It will be noted that, while the Coulomb excitation determines the general shape and magnitude of the angular distribution, the addition of the (real) nuclear potential completely changes the phase of the oscillations. This phase change is essential to fit the data. The imaginary potential only plays a role at extreme back angles; it is, however a determining factor in the exponential fall off of the elastic scattering cross section.

The importance of Coulomb excitation in the inelastic scattering has two immediate consequences: (i) a large number (~300) of partial waves must be included, and (ii) the integrals for *all* partial waves must be carried out to large radii. Various authors[10, 13] have resolved the first problem by using a semiclassical calculation[14] of pure Coulomb excitation beyond a certain strategic value of l_s and a conventional DWBA code below this value. In our case, for example, the nuclear excitation vanishes for $l \sim 60$. It should be noted, however, that Coulomb excitation at large radii can be significant even for relatively small values of l.

Figure 8 shows the absolute value of the S-matrix elements $|S_{I,l=I}|$ for a typical case, where the integration has been carried out to 30, 50, or 60 fm. The distribution has two maxima, one from nuclear effects ($l=25$), and one from Coulomb ($l=33$), with an interference region straddling the two. It will be noted that the truncation of the integrals causes differences not only for large values of l (cutting off the calculation at 149, 256, and 311 partial waves, respectively), but also in the region of Coulomb-nuclear interference (although these are small.)

The significance of these changes can be seen in Fig. 9, which plots the cross sections corresponding to the three cases in Fig. 8. The striking differences in the small-angle behavior represent the effect of the large-l cutoff. It can be

TABLE II. Deformation parameters from the coupled-channels analysis. The numbers cited for β_2^N and β_2^C are those which would give the same values for the products $\beta_2^N R_0$ and $\beta_2^C R_0^2$, respectively, that were found in our search, but with a radius $R_0 = 1.2 A_T^{1/3}$ fm. They may thus be directly compared with the Coulomb excitation values from Ref. 11.

System	β_2^N (This work)	β_2^C (This work)	β_2 (Ref. 11)
$^{64}Ni + ^{16}O$	0.222	0.169	0.192
$^{72}Ge + ^{16}O$	0.214	0.222	0.247
$^{74}Ge + ^{16}O$	0.265	0.267	0.290
$^{76}Ge + ^{16}O$	0.228	0.256	0.271
$^{72}Ge + ^{18}O$	0.236	0.219	0.247
$^{74}Ge + ^{18}O$	0.265	0.266	0.290
$^{76}Ge + ^{18}O$	0.231	0.262	0.271

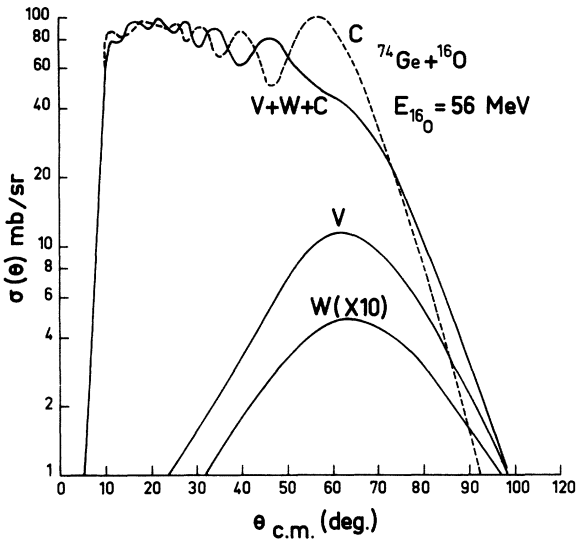

FIG. 7. Contributions to the inelastic cross section from Coulomb excitation (C) and excitation by the real (V) and imaginary (W) potentials. The curve labeled "$V + W + C$" represents the total cross section resulting from the coherent sum of the three components.

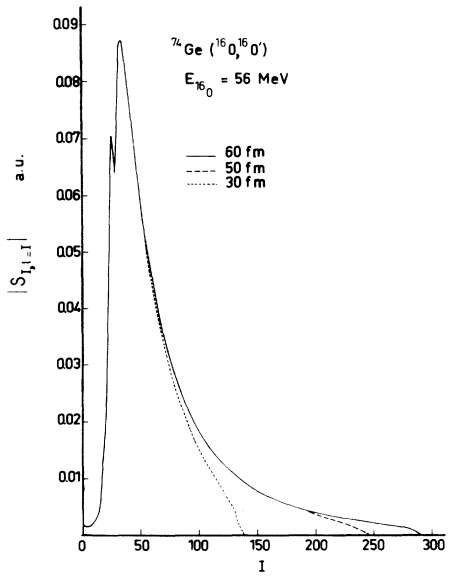

FIG. 8. Magnitudes of the S-matrix elements for the inelastic scattering as a function of the total channel spin I for the partial waves $l = I$. The S matrix is expressed in helicity representation. The radii indicated are the matching radii in the calculation, where the integration is stopped and boundary conditions applied.

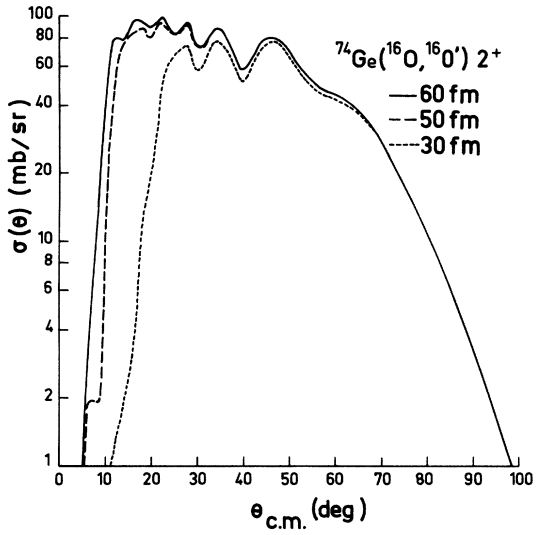

FIG. 9. Angular distributions resulting from the three calculations in Fig. 8. (Note that the potential used in Figs. 7–9 differs slightly from the $^{16}O+^{74}Ge$ potential quoted in Table I.)

seen, however, that, particularly for the 30 fm case, significant differences persist even out to the grazing angle. This is due to the fact the oscillatory behavior is extremely sensitive to the relative magnitudes and phases of the Coulomb and nuclear amplitudes.

In light of these considerations, all of our parameter searches were carried out with a matching radius, R_m = 50 fm. After a best fit was found, the calculation was repeated (without a search) with R_m = 60 fm. In all cases, the small differences at forward angles were insignificant within the precision of the data.

C. Ambiguities

Since the elastic scattering angular distribution alone cannot uniquely determine an optical potential, various authors have attempted to find "constants" that would define a given family of continuously ambiguous potentials. One of the earliest approaches, applied originally to α-particle scattering, was developed by Igo,[1] who noted that, for the large radii that influence elastic scattering, a Woods-Saxon potential becomes a simple exponential, i.e.:

$$V(r) = V_0(1+\exp(r-R_V)/a_V)^{-1}$$
$$\approx V_0\exp(R_V/a_V)\exp(-r/a_V)\,. \quad (1)$$

Thus, for a given value of a_V, any potential having the same value of

$$I(a_V) = \ln V_0 + R_V/a_V \quad (2)$$

will have the same tail, and hence give the same elastic scattering angular distribution. A corresponding relation holds for the imaginary potential. This relation has been recently confirmed[15] for ^{16}O elastic scattering of nickel isotopes over three orders of magnitude for V_0, and one and one-half orders for W_0, in a four-parameter search.

The chief limitation of the Igo prescription is that it only relates potentials with the same diffusivity. A more general comparison can be made by calculating the radius and height of the Coulomb barrier. It has been shown[15,16] that for scattering at energies comparable to the barrier height, these quantities will define a set of potentials giving equivalent fits. For the case of a constant diffusivity, the requirement that the barrier height V_b be constant reduces to the Igo ambiguity.[15]

TABLE III. Parameters defining the potentials of Table I according to the schemes of Satchler (Ref. 17) and of West, Kemper, and Fletcher (Ref. 15). The quantities are defined in the text.

System	Critical values (Ref. 17) $L_{1/2}$	$r_{1/2}$ [a]	$V(D_{1/2})$	$W(D_{1/2})$	Barrier parameters (Ref. 15) r_b [b]	V_b
$^{64}Ni+^{16}O$	28	1.54	1.40	0.28	1.52	30.7
$^{72}Ge+^{16}O$	27	1.56	1.11	0.33	1.52	34.3
$^{74}Ge+^{16}O$	27	1.55	1.13	0.33	1.52	34.3
$^{76}Ge+^{16}O$	28	1.55	1.08	0.32	1.51	34.2
$^{72}Ge+^{18}O$	28	1.58	1.00	0.30	1.52	33.6
$^{74}Ge+^{18}O$	30	1.59	0.91	0.30	1.52	33.5
$^{76}Ge+^{18}O$	31	1.59	0.92	0.53	1.52 [c]	33.5 [c]

[a] $D_{1/2}=r_{1/2}(A_T^{1/3}+A_P^{1/3})$ [cf. Eq. (3)].
[b] $R_{\text{barrier}}=r_b(A_T^{1/3}+A_P^{1/3})$.
[c] Extremely flat barrier; the depth of this potential is too small. V_0=12.33 MeV.

A third formulation for equivalent potentials has been proposed by Satchler.[17] One can define the critical l, $L_{1/2}$, as the value for which the transmission coefficient T_l is equal to $\frac{1}{2}$. Then, by using the semiclassical equation for the distance of closest approach,

$$D = (\eta/k)\{1 + [1 + (l/\eta)^2]^{1/2}\} , \quad (3)$$

where η is the Coulomb parameter and k is the wave number, one can find the value $D_{1/2}$ corresponding to this critical l. All equivalent potentials should have roughly the same values of $V(D_{1/2})$ and $W(D_{1/2})$.

Table III lists the parameters of these two latter formulations for the potentials of Table I. (The Igo prescription, above, is not relevant here due to the differing values of a.) As can be seen, all of these potentials give essentially the same values, and thus belong to the same family. This is not surprising, since they describe similar systems and were derived from the same starting potential for the search.

All the above ambiguities refer to elastic scattering. Since inelastic scattering involves a process interior to the nucleus, it should therefore be sensitive to a different region of the optical potential, and hence lift some of the ambiguity. Due to the cost of the coupled-equations calculation, it was necessary to limit the scope of these investigations. A few points are adequate, however, to show the result.

We have chosen to investigate the Igo ambiguity, which is extremely well reproduced for heavy-ion elastic scattering.[15] Table IV presents the result of a restricted search conducted as follows, for the case of $^{16}O + ^{74}Ge$ scattering: The value of V_0 was offset from its value at the minimum χ^2, then fixed; a_V and a_W were fixed. A search was performed on r_V, r_W, W, and β_2. The parameter W was allowed to vary since, as opposed to the case of a four-parameter fit, the ratio W/V is not necessarily constant (cf. Ref. 15). As can be seen, over a fairly small range of values of V (a factor of 3), significant changes appear in the Igo constant. In addition, the value of χ^2 begins to mount rapidly as V is increased. Thus, due to the additional constraints imposed by fitting the inelastic scattering, the χ^2 surface now has a local minimum, rather than a long "valley." This is exactly the result hoped for.

TABLE IV. Investigation of the Igo ambiguity for the $^{16}O + ^{74}Ge$ potential of Table I. The Igo parameter $I(a)$ is defined in Eq. (2) of the text. Note that this parameter has a logarithmic dependence on V, and thus small differences are significant. $a_0 = 0.43$ fm, $a_i = 0.42$ fm.

V (MeV)	r_0 (fm)	$I(a_0)$	W (MeV)	r_i (fm)	$I(a_i)$	W/V	χ^2_{tot}/N
15.0	1.40	24.7	32.7	1.28	23.9	2.18	3.0
24.5	1.36	24.6	36.7	1.26	23.7	1.49	3.0
35.0	1.35	24.8	47.7	1.26	24.0	1.36	5.2
50.0	1.36	25.3	38.7	1.37	25.6	0.77	11.6

IV. CONCLUSIONS

The observed cross sections for the elastic and inelastic scattering of oxygen ions from the nickel and germanium targets have been simultaneously reproduced by a coupled-equations calculation. The shapes of the inelastic angular distributions are determined largely by Coulomb excitation, while the fine structure is the result of Coulomb nuclear interference. Thus, the Coulomb contribution must be calculated accurately by employing an adequate number of partial waves and integrating to sufficiently large radii. The calculated values of β_2 are in good agreement with the published results from Coulomb excitation.

While the possibility of discrete ambiguities has not been entirely ruled out, it appears that the potentials determined by this study are unique. This is a marked improvement over the case of elastic scattering alone. In addition, since inelastic excitation of the 2^+ levels is explicitly calculated in the formalism, rather than implicitly included in the potentials, the optical parameters derived are more suitable for use in a CCBA calculation of the transfer reactions.[7]

The authors would like to thank Professor John Blair for his helpful discussions, and Dr. Jacques Raynal for his assistance with his code. One of the authors (M. E. C.) wishes to thank Dr. E. Cotton and the members of his service for their hospitality during his stay at Saclay.

*Current address: Tandem Accelerator Laboratory (E 1), University of Pennsylvania, Philadelphia, Pennsylvania, 19174.

[1]G. Igo, Phys. Rev. Lett. 1, 72 (1958); Phys. Rev. 117, 1665 (1959).
[2]G. H. Rawitscher, Nucl. Phys. 83, 259 (1966).
[3]M. C. Lemaire, M. C. Mermaz, H. Sztark, and A. Cunsolo, Phys. Rev. C 10, 1103 (1974).

[4]W. Henning, D. G. Kovar, B. Zeidman, and J. R. Erskine, Phys. Rev. Lett. 32, 1015 (1974).
[5]M. J. LeVine, A. J. Baltz, P. D. Bond, J. D. Garrett, S. Kahana, and C. E. Thorn, Phys. Rev. C 10, 1702 (1974); A. J. Baltz, P. D. Bond, J. D. Garrett and S. Kahana, Phys. Rev. C 12, 136 (1975).
[6]E.g., P. E. Hodgson, *Nuclear Reactions and Nuclear Structure* (Clarendon, Oxford, 1971), pp. 87–140.
[7]R. J. Ascuitto and N. K. Glendenning, Phys. Lett. 47B, 332 (1973); T. Tamura, K. S. Low and T. Udagawa, *ibid*. 51B, 116 (1974); M. E. Cobern, M. C. Lemaire, K. S. Low, M. C. Mermaz, H. Sztark, T. Udagawa, and T. Tamura (unpublished).
[8]J. Raynal, Saclay Report No. DPh-T/71-48, 1971 (unpublished).
[9]H. Padé, Ann. Sci. École Norm. Sup. (Paris) 9, 1 (1892); 16, 395 (1899).
[10]P. R. Christensen. I. Chernov, E. E. Gross, R. Stokstad, and Vidabaek, Nucl. Phys. A207, 433 (1973).
[11]A. H. Wapstra, Nucl. Data A1, 21 (1965).
[12]J. L. C. Ford, Jr., K. S. Toth, D. C. Hensley, R. M. Gaedke, P. J. Riley, and S. T. Thornton, Phys. Rev. C 8, 1912 (1973).
[13]K. E. Rehm, H. J. Körner, R. Richter, H. P. Rother, J. P. Schiffer, and H. Spieler (unpublished).
[14]M. Samuel and U. Smilansky, Comput. Phys. Commun. 2, 1455 (1971).
[15]L. West, Jr., K. W. Kemper, and N. R. Fletcher, Phys. Rev. C 11, 859 (1975).
[16]M. C. Bertin, S. L. Tabor, B. A. Wadton, Y. Eisen, and G. Goldring, Nucl. Phys. A167, 216 (1971).
[17]G. R. Satchler, in *Proceedings of the International Conference on Reactions between Complex Nuclei, Nashville, Tennessee, June, 1974*, edited by R. L. Robinson, F. K. McGowan, J. B. Ball, and J. H. Hamilton (North-Holland, Amsterdam/American Elsevier, New York, 1974), Vol. 2, p. 171.